Author(s): Pesola, M. & von Boehm, J. & Mattila, T. & Nieminen, Risto M.

Title: Computational study of interstitial oxygen and vacancy-oxygen complexes in silicon

Year: 1999

Version: Final published version

Please cite the original version:

Pesola, M. & von Boehm, J. & Mattila, T. & Nieminen, Risto M. 1999. Computational study of interstitial oxygen and vacancy-oxygen complexes in silicon. Physical Review B. Volume 60, Issue 16. 11449-11463. ISSN 1550-235X (electronic). DOI: 10.1103/physrevb.60.11449.

Computational study of interstitial oxygen and vacancy-oxygen complexes in silicon

M. Pesola*
Laboratory of Physics, Helsinki University of Technology, P.O. Box 1100, FIN-02015 HUT, Finland

J. von Boehm†
LTAM, Helsinki University of Technology, P.O. Box 1100, FIN-02015 HUT, Finland

T. Mattila‡
Laboratory of Physics, Helsinki University of Technology, P.O. Box 1100, FIN-02015 HUT, Finland and National Renewable Energy Laboratory, Golden, Colorado 80401

R. M. Nieminen§
Laboratory of Physics, Helsinki University of Technology, P.O. Box 1100, FIN-02015 HUT, Finland
(Received 22 January 1999; revised manuscript received 2 June 1999)

The formation and binding energies, the ionization levels, the structures, and the local vibrations of O_i, O_{2i}, O_{3i}, VO, VO_2, and V_2O (V=vacancy) in silicon are calculated using a self-consistent total-energy pseudopotential method. The most important results are as follows: The ionization levels and associated structures are given for VO and V_2O as well as the local vibration modes for the negative charge states of VO. The experimental frequency of O_i at 517 cm^{-1} is associated tentatively with an oxygen-induced silicon mode of weakly interacting O_i's. We find two competing structures for O_{2i}: the staggered configuration and the skewed O_i-Si-Si-O_i configuration with the binding energies of 0.2 and 0.1 eV, respectively. The experimental frequencies of O_{2i} at 1060, 1012, 690, and 556 cm^{-1} are found to originate from the staggered O_{2i}. The experimental frequency of O_{2i} at 1105 cm^{-1} is found to originate from the skewed O_i-Si-Si-O_i configuration of O_{2i}. The calculated effects of pressure on the structures and local vibration frequencies (Grüneisen parameters) of O_i and O_{2i} are presented. [S0163-1829(99)06535-2]

I. INTRODUCTION

When crystalline silicon is grown by the Czochralski (Cz) method it is contaminated by oxygen dissolving from the surrounding quartz crucible. Cz-grown silicon can contain approximately 10^{18} oxygen atoms in one cubic centimeter. Their presence can be very useful in the fabrication of silicon wafers because the oxygen atoms are able to increase the mechanical strength of silicon material and to act as gettering centers of other impurities. However, oxygen in as-grown Cz silicon appears supersaturated and hence the oxygen distribution is highly inhomogeneous. Heat treatments are therefore used to homogenize the oxygen distribution. However, when oxygen atoms become mobile at temperatures $> 350\,^{\circ}C$ they begin to cluster. A related (harmful and at the same time interesting) phenomenon is the appearance of the so-called thermal donors.[1] These are commonly believed to contain a core to which oxygen atoms aggregate resulting in a family of closely related donors. Several families of thermal donors are known: thermal double donors, shallow thermal donors, and new thermal donors.[1–4] At least sixteen thermal donor members have been observed.[2,5]

Individual oxygen atoms occupy interstitial bond-center (BC) positions in silicon.[6] The interstitial oxygen atoms O_i are known to diffuse by hopping between the neighboring BC sites with an activation energy of 2.53 eV in a large temperature range of 300–1200 °C.[6,7] However, aggregation takes place with a much lower activation energy of about 1.8 eV.[8] Oxygen-containing fast diffusing species (FDS's) are therefore needed to explain the aggregation.[9,10]

Several experimental methods have given valuable information about the oxygen defects. The electron paramagnetic resonance (EPR), electron-nuclear double resonance (ENDOR), and positron annihilation (PA) methods give information about wave functions and atomic structures, the deep level transition spectroscopy (DLTS) and photoconductivity about ionization levels, and infrared (IR) spectroscopy about local vibrations (LV's).[11,12] However, despite these efforts as well as several systematic theoretical calculations,[13–18] the aggregation processes and the atomic structures of the thermal donor cores are not yet well understood. The understanding certainly rests on firm knowledge of the properties of the basic oxygen complexes. For example, the formation of an interstitial oxygen pair O_{2i} as well as the formation of a vacancy-dioxygen complex VO_2 play an important role in understanding aggregation. Further, it has been suggested that VO and O_{2i} could be FDS's.[10,19] To gain a better understanding of the physical behavior of oxygen in silicon we present here a systematic study of the basic interstitial oxygen and vacancy-oxygen complexes O_i, O_{2i}, O_{3i}, VO, VO_2, and V_2O in silicon using state-of-art total-energy pseudopotential (PP) methods. The properties to be considered are the formation and binding energies, the ionization levels, the structures and bonding, as well as the LV's.

The format of this paper is as follows. The methods are presented in Sec. II. Results for energy quantities, structures, bonding, and local vibrations as well as the related discus-

sions are presented in Sec. III. The conclusions are drawn in Sec. IV.

II. METHODS

A. Computational methods

We use the density-functional theory (DFT) (Ref. 20) in the local density (LD) (Ref. 21) and local mass (LM) (Ref. 22) approximations as well as the spin-polarized DFT (Refs. 20,23) in the local spin-density (LSD) (Ref. 23) approximation. Our calculations are performed using a self-consistent total energy PP method. The Perdew-Zunger (PZ) (Ref. 24) parametrization of the Ceperley-Alder data[25] is used for the exchange-correlation energy.

For silicon we use the norm-conserving Hamann PP.[26] The PP is of the fully separable Kleinman-Bylander form[27] and the *s* component is used as the local one. For oxygen we use the ultrasoft Vanderbilt PP.[28] The valence-electron wave functions are expanded in a plane-wave basis set up to a kinetic-energy cutoff of 28 Ry. The Vanderbilt PP was tested for an oxygen dimer (O_2) by calculating the bond length and vibrational frequency of O_2. We find a bond length of 1.217 Å and a vibrational frequency of 1557 cm^{-1} which are close to the experimental values of 1.2074 Å and 1554.7 cm^{-1},[29] respectively.

We use mostly a lattice constant of 10.185 $a_0 = 5.390$ Å which is obtained from a 2 atom-site supercell calculation for bulk silicon with 4^3 Monkhorst-Pack (MP) **k** points.[30] However, in some cases the addition of oxygen atoms in the supercell can cause considerable internal pressure which is removed by increasing the lattice constant appropriately.

We use mostly the MP 2^3 **k**-point sampling and 32 and 64 atom-site supercells but occasionally also a 128 atom-site supercell with the Γ point in our calculations. These supercell sizes give a sufficient accuracy for total energy calculations. For example, the chemical potential for silicon using the 32 atom-site supercell is by 2.7 meV and the 64 atom-site supercell by 1.3 meV higher than the well-converged value obtained with the 2 atom-site supercell and the MP 6^3 **k**-point sampling. However, these supercell sizes may be less satisfactory for the structures of the defects. For example, similar supercell calculations for the silicon vacancy and divacancy have shown that a sufficient convergence in the structure is not reached before the 216 atom-site supercell.[31,32] The main reason for the relatively slow convergence lies in the spurious defect-defect interactions along the [110] directional chains in silicon formed by periodically repeating the supercell. Another supercell-size-related matter is the dispersion of the one-electron states. When using 32 and 64 atom-site supercells the dispersion of one-electron states is still of the order of the calculated forbidden energy gap and there is a risk that the bands of the gap levels cross the valence band maximum (or conduction band minimum) at some **k** points, worsening the result. All calculations have been performed in a massively parallel CRAY-T3E system using the `FINGER` code.[33]

B. Computation of energy quantities

The total energy in our calculations is of the form

$$E_D[\{\phi_{i\sigma}\},\{\mathbf{R}_I\}] = \sum_{i\sigma} f_{i\sigma} \left\langle \phi_{i\sigma} \left| -\frac{1}{2}\nabla^2 + V_{\mathrm{NL}} \right| \phi_{i\sigma} \right\rangle + \frac{1}{2}\int\int d\mathbf{r}\, d\mathbf{r}' \frac{n(\mathbf{r})n(\mathbf{r}')}{|\mathbf{r}-\mathbf{r}'|} + E_{\mathrm{xc}}[n_\uparrow(\mathbf{r}), n_\downarrow(\mathbf{r})] + \int d\mathbf{r}\, V^{\mathrm{ion}}(\mathbf{r}) n(\mathbf{r}) + U(\{\mathbf{R}_I\}) \quad (2.1)$$

where $n(\mathbf{r}) = n_\uparrow(\mathbf{r}) + n_\downarrow(\mathbf{r})$ is the total electron density consisting of the spin-up and -down densities. $f_{i\sigma}$ is an occupation number for the spin-orbital $\phi_{i\sigma}$, $f_{i\sigma} = 0$ or 1. The first term on the right-hand side consists of the kinetic energy of the noninteracting electrons and the nonlocal contribution from the pseudopotential construction. The second term is the Hartree energy of the electrons and the third term the exchange-correlation energy. The last two terms represent the Coulombic interaction energy between the local ionic pseudopotential cores and the valence electron density and the Coulombic energy between the ion cores at the positions $\mathbf{R}_I$.[28]

In our calculations spin-polarization is taken into account in those cases where the defect has an unpaired number of electrons. In other cases the usual unpolarized LD or LM approximation is used unless otherwise stated.

The formation energy of a defect in the charge state Q is given by[34–37]

$$E_f(Q) = E_D(Q) + Q(E_v + \mu_e) - \sum_s n_s \mu_s, \quad (2.2)$$

where Q is the charge of the supercell in units of elementary charge, E_v is the valence band maximum, and μ_e is the electron chemical potential relative to the valence band maximum. The constituents of the last summation, n_s and μ_s are the number of type *s* atoms in the supercell and the atom chemical potential, respectively.

The values for the valence band maximum and the silicon atom chemical potential are obtained from a defect-free bulk calculation with the same supercell size and **k**-point sampling. The low-temperature form of SiO_2, α quartz, is used to get the chemical potential of an oxygen atom. The unit cell of α quartz contains three silicon and six oxygen atoms. The chemical potential is obtained from the calculated total energy E_D using the known silicon chemical potential as follows: $\mu_O = (E_D - 3\mu_{Si})/6$.

The valence band maximum E_v has been corrected using the average potential correction[37] as

$$E_v = E_v(\mathrm{bulk}) + [V_{\mathrm{ave}}(\mathrm{defect}) - V_{\mathrm{ave}}(\mathrm{bulk})]. \quad (2.3)$$

The average potential correction is needed because of the limited supercell size. Basically this correction aligns the energies so that comparison between different charge states can be made.

The ionization level (Q'/Q) for a given defect is defined as the position of μ_e in the band gap where the stablest charge state changes from Q' to Q. The ionization levels are derived from the total energy and are therefore more reliable than the one-electron eigenvalues which are more directly

influenced by the underestimation of the band gap. An ionization level can be obtained by solving μ_e from the equation

$$E_D(Q)+Q(E_V^Q+\mu_e)=E_D(Q')+Q'(E_V^{Q'}+\mu_e). \tag{2.4}$$

C. Computation of local vibrations

In the harmonic approximation the total energy is written as a Taylor series of the atomic displacements. The coupling constants are obtained as numerical derivatives of the Hellman-Feynman forces

$$\Phi_{n\alpha i}^{m\beta j}\equiv\frac{\partial}{\partial R_{n\alpha i}}\left(\frac{\partial E_D}{\partial R_{m\beta j}}\right) \tag{2.5}$$

where n and m indicate the supercell, α and β the atom in the corresponding supercell and i and j the Cartesian direction. The dynamical matrix is defined as[38]

$$D_{\alpha i}^{\beta j}(\mathbf{q})\equiv\sum_m\frac{1}{\sqrt{M_\alpha M_\beta}}\Phi_{0\alpha i}^{m\beta j}e^{i\mathbf{q}\cdot\mathbf{R}_m}. \tag{2.6}$$

The LV's become independent of $\mathbf{q}$ for a sufficiently large supercell. Then one can neglect the sum over m in Eq. (2.6) and calculate the LV's as eigenvalues of the dynamical matrix at $\mathbf{q}=0$:

$$D_{\alpha i}^{\beta j}=\frac{\Phi_{0\alpha i}^{0\beta j}}{\sqrt{M_\alpha M_\beta}}. \tag{2.7}$$

The validity of this approximation has been tested by calculating the LV modes with different supercell sizes. It turns out that the 32 atom-site supercell is sufficient in calculating the LV's.[39]

In practice the LV calculations are performed using the procedure and program by Köhler *et al.*[40] In our calculations every atom in the supercell is slightly displaced in the six Cartesian directions. After the displacement the electronic structure for this configuration is reoptimized and the resulting Hellman-Feynman forces are calculated. The coupling constants are then calculated by finite differences using these forces and displacements[40] and the dynamical matrix is formed using Eq. (2.7). The LV frequencies and the corresponding normal modes can then be obtained by diagonalizing the dynamical matrix.[40]

We calculate the LV frequencies for the neutral *V*O also using microcanonical (constant NVE) molecular dynamics (MD) and the velocity-Verlet algorithm that conserves the total energy.[41] The simulation is adiabatic in the sense that the electronic structure is allowed to relax between the moves, keeping the electrons near the Born-Oppenheimer surface. However, the inaccuracies in the Hellman-Feynman forces when the electronic structure is not exactly on the Born-Oppenheimer surface cause a small shift in the total energy during the simulation. This shift—insignificant for our purposes—is 0.5 eV for the whole 32 atom-site supercell during the whole simulation period of 2 ps. The timestep for ionic movements used in our simulations was 3.6 fs. The MD run was started from the relaxed structure of *V*O obtained with the 32 atom-site supercell. In the beginning of the MD run the system was allowed to thermalize. The peaks of the LV modes for *V*O in the vibration density of states can be obtained directly from the power spectrum which is calculated by taking the real part of the discrete Fourier transform of the velocity autocorrelation function

$$Z(t)=\frac{\sum_{s,i}\mathbf{v}_i(t+s)\cdot\mathbf{v}_i(s)}{\sum_{s,i}\mathbf{v}_i(s)\cdot\mathbf{v}_i(s)}. \tag{2.8}$$

For a more complete description of the method, see, for example, Ref. 42.

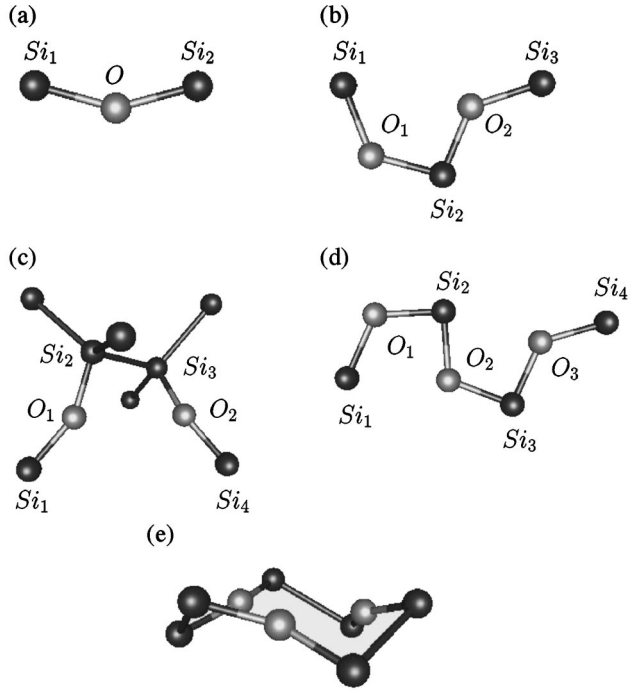

FIG. 1. The calculated structures of the interstitial oxygen complexes studied. Dark spheres represent silicon atoms, light gray spheres oxygen atoms. (a) Interstitial oxygen, (b) staggered oxygen dimer (S), (c) skewed O_i-Si-Si-O_i configuration of oxygen dimer (SK), (d) staggered oxygen trimer (S), (e) ringlike oxygen trimer (R).

III. RESULTS AND DISCUSSION

A. Energies and structures

1. Interstitial oxygen complexes

Figure 1 shows the calculated configurations for the interstitial oxygen complexes. The calculated structure for O_i in Fig. 1(a) agrees with the widely accepted model for O_i where the oxygen atom breaks the [111]-directional bond and is displaced off from the actual BC to form a ''puckered'' structure.[6,43] O_{2i} appears in two competing configurations: The staggered configuration in Fig. 1(b) found by Needels *et al.*[15] consists of two O_i's bonded to a common silicon atom (Si_2). The skewed O_i-Si-Si-O_i configuration in Fig. 1(c) found by Öberg *et al.*[44] consists of two more separated O_i's such that Si_1-O_1-Si_2 and Si_3-O_2-Si_4 projected on a plane perpendicular to Si_2-Si_3 form roughly an angle of 60°.

TABLE I. Formation energies (eV) of the interstitial oxygen complexes as calculated from Eq. (2.2). The results are obtained with the lattice constant of 5.39 Å of a defect-free bulk silicon. SK, S, and R denote the skewed O_i-Si-Si-O_i, the staggered, and the ringlike configurations, respectively. The Γ point **k** sampling is used in calculating with the supercell of 128 Si atoms. The oxygen chemical potential is obtained from the α quartz that is the low-temperature form of SiO_2.

	No. Si atoms	O_i	O_{2i} (S)	O_{2i} (SK)	O_{3i} (S)	O_{3i} (R)
E_f	128	1.1	2.0	2.1		
	32	1.8	3.0	3.4	~4.1	~4.9

Two configurations of O_{3i} are considered in the present study. The staggered configuration in Fig. 1(d) found by Needels *et al.*[15] is a natural extension of the staggered O_{2i}: three O_i's are bonded to two common silicon atoms (Si_2, Si_3), the whole Si_1-O_1-Si_2-O_2-Si_3-O_3-Si_4 complex belongs to one of the {110} planes. The ringlike O_{3i} in Fig. 1(e) is a natural extension of the skewed O_i-Si-Si-O_i configuration in Fig. 1(c): the three O_i's are always separated by two silicon atoms (six silicon atoms altogether).

We consider next the formation and binding energies of the above interstitial complexes. Table I lists the calculated formation energies and Table II the calculated binding energies together with other calculations[15,18,45–47] and experiments.[10] The staggered and the skewed O_i-Si-Si-O_i configurations of O_{2i} have very close binding energies. The binding energies of two O_i's calculated with a 32 atom-site supercell equal 0.2 eV for the skewed O_i-Si-Si-O_i structure and 0.6 eV for the staggered configuration. However, in an extended calculation using a larger supercell of 128 atom sites and the Γ point **k** sampling we find that the staggered configuration is only by 0.1 eV more stable than the skewed O_i-Si-Si-O_i configuration, the binding energies being equal to 0.2 and 0.1 eV, respectively. These binding energies agree closely with the values of 0.3 and 0.2 eV obtained from IR absorption experiments for two different oxygen dimer structures.[10]

The binding energies of the O_{3i} structures given in Table II are probably overestimated because of the limited supercell size. We can roughly estimate the binding energy of the staggered O_{3i} by comparing the formation energies of O_i and O_{2i} in different supercells. The formation energies are overestimated by ~60% with the 32 atom-site supercell (Table I). If this would be the case also with O_{3i} then the formation energy would be only 2.6 eV. This would lead to a binding energy of 0.7 eV when O_{3i} is formed from three isolated O_i's.

According to our calculations O_i's show a clear tendency to form staggered chains in the $\langle 110 \rangle$ directions. This tendency can be seen in two ways. First, the formation energy per O_i decreases from O_i to O_{2i} to O_{3i} (Table I). Second, the binding energy per O_i increases from 0.3 eV for O_{2i} to 0.4 eV for O_{3i} (Table II). This behavior is also consistent with experiments according to which oxygen atoms cluster in a planar form resulting in long chains of oxygen atoms.[11] Especially it is known that the TD's in silicon have such long chains in {110} planes.[11]

As to the other calculations listed in Table II our calculated values agree reasonably well with the values given by Needels *et al.*[15] and Chadi[18] obtained using similar methods to ours. Kelly[45] finds that O_{2i} is unstable. Saito and Oshiyama[46] find that the stabilization energy for O_{3i} equals 11.7 eV which is less than three times the stabilization energy of 4.6 eV for O_i. Snyder *et al.*[47] find a slightly bound O_{2i}. Öberg *et al.*[44] find that the skewed O_i-Si-Si-O_i configuration is by 0.14 eV more stable than an O_{2i} configuration consisting of two neighboring O_i's bound to a common silicon atom, whereas Ewels *et al.*[48] found earlier using the same method that the latter configuration is more stable by 0.68−0.82 eV. Thus, considerable differences exist between different calculations.

TABLE II. Binding energies of the interstitial oxygen complexes (eV). The methods included are the pseudopotential (PP), Green's matrix (G), and semiempirical (MINDO/3) method. SC, C, and CC denote supercell, (*H*-terminated) cluster, and cyclic cluster, respectively. S and SK denote the staggered and the skewed O_i-Si-Si-O_i configuration, respectively. The number after SC, C, or CC gives the number of Si atoms. The Γ point **k** sampling is used in calculating with the supercell of 128 Si atoms. The lattice constant of 5.39 Å of a defect-free bulk silicon is used in our calculations.

	Method	O_{2i} vs $2\times O_i$	O_{3i} vs $3\times O_i$	O_{3i} vs $O_{2i}+O_i$
This work	PP SC 128	0.2 (S)		
	PP SC 128	0.1 (SK)		
	PP SC 32	0.6 (S)	1.3 (S)	0.8 (S)
	PP SC 32	0.2 (SK)		
Chadi[a]	PP SC 32		0.7 (S)	0.4 (S)
Needels *et al.*[b]	PP SC 16-64	1.0 (S)	2.0 (S)	1.0 (S)
Kelly[c]	G	<0		
Saito and Oshiyama[d]	PP C 11		<0	
Snyder *et al.*[e]	MINDO/3 CC 47	0.1		
Experiment[f]		0.3 and 0.2		

[a]Reference 18.
[b]Reference 15.
[c]Reference 45.
[d]Reference 46.
[e]Reference 47.
[f]Reference 10.

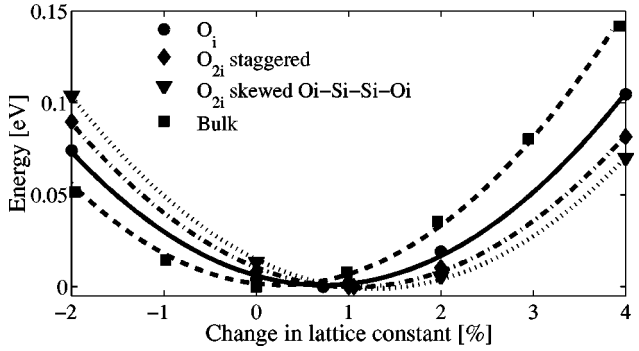

FIG. 2. Total energy of primitive unit cell as a function of the lattice parameter for the oxygen interstitial complexes. The changes in the lattice constant are calculated from the defect-free bulk lattice constant of 5.39 Å . Black filled circles represent the results for O_i, diamonds for the staggered O_{2i}, triangles for the skewed O_i-Si-Si-O_i configuration of O_{2i}, and squares for the defect-free bulk. Lines are drawn to guide the eye. The defect-free bulk energies are obtained with a 2 atom-site supercell and 6^3MP **k**-point sampling. The energy values for the 32 atom-site supercell used in our calculations are divided by 16 so that comparisons to the 2 atom-site results are possible.

Our results in Tables I and II were obtained using the lattice constant of defect-free bulk silicon. Figure 2 shows the calculated total energies of the defect supercells and defect-free bulk silicon as a function of the lattice constant. The increase in the lattice constant to minimize the pressure in the supercell does not change the total energies of the defects significantly. This effect is of the order of a meV in the total energy of the primitive unit cell (two atoms) but may have significant effects in the vibrational frequencies and details in the defect geometries. According to Fig. 2 about 1% increase in the lattice constant is needed to remove the internal pressure. Our theoretical value for the bulk modulus for defect-free bulk silicon is 1.0 Mbar that matches the experimental value of 0.98 Mbar (Ref. 49) very closely. Increasing the number of oxygen atoms in the supercell lowers the value to 0.91 Mbar in the case of O_i and to 0.86 Mbar in the case of O_{2i} in both staggered and skewed O_i-Si-Si-O_i configuration. Thus the direct effect of adding oxygen is to soften the silicon crystal. The increase in mechanical strength is then due to indirect mechanisms like preventing motions of dislocations. The pressure in the supercell when using the defect-free bulk lattice constant is 16 kbar for O_i, 24 kbar for the staggered configuration of O_{2i}, and 31 kbar for the skewed O_i-Si-Si-O_i configuration of O_{2i}.

Consider next the structures of the interstitial oxygen complexes in Fig. 1 in more detail. The calculated structures of O_i are given in Table III together with previous theoretical studies[16,18,46,48,50–54] and experimental results.[43] From experiments applied pressure is known to decrease the Si-O_i-Si angle.[55] We find the same behavior which is shown in Fig. 3(a). The internal pressure of a defect supercell (and the spurious O_i-O_i interactions) can also be decreased by increasing the size of the supercell. We indeed find the opening of the Si-O_i-Si angle with increasing the size of the supercell [Fig. 3(b)]. When the pressure in a 32 atom-site supercell is relieved by increasing the lattice constant or when the pressure is diminished by increasing the size of the supercell up to 128 atom-sites the Si-O_i-Si bond angle is found to increase.

TABLE III. Structures of O_i. The methods included are the pseudopotential (PP), Hartree-Fock (HF), Green matrix (G), and semiempirical (MINDO/3, PRDDO) method. SC, C, and CC denote supercell, (*H*-terminated) cluster, and cyclic cluster, respectively. The number after SC, C, or CC gives the number of Si atoms. The Γ point **k** sampling is used in calculating with the SC of 128 Si atoms. The lattice constant of 5.39 Å of a defect-free bulk silicon is used in our calculations except for the first values obtained with the 32 atom-site SC which are free from pressure.

	Method	Si-O_i-Si (deg.)	Si-O_i (Å)
This work	PP SC 128	154	1.63
	PP SC 32	154,150	1.62,1.62
	PP SC 8	127	1.65
Chadi[a]	PP SC 32	144	1.65
Ewels *et al.*[b]	PP C ~60		1.63
Artacho *et al.*[c]	HF C 8	~180	~1.6
Jones *et al.*[d]	PP C 44	172	1.59
Kelly and Car[e]	G	140	1.77
Deák *et al.*[f]	MINDO/3 CC 47	180	1.61
Estreicher[g]	PRDDO C 26,35	164	1.57
Saito and Oshiyama[h]	PP C 10	157	1.68
Martinez *et al.*[i]	HF C 8	162	1.62
Experiment[j]		162	

[a]Reference 18. [f]Reference 16.
[b]Reference 48. [g]Reference 53.
[c]Reference 50. [h]Reference 46.
[d]Reference 51. [i]Reference 54.
[e]Reference 52. [j]Reference 43.

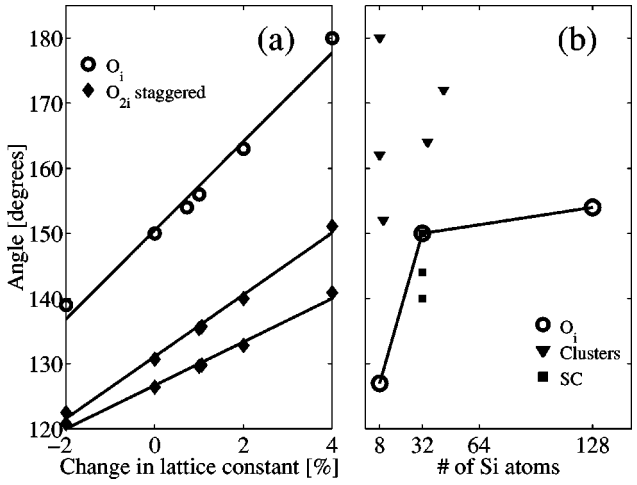

FIG. 3. (a) The Si-O_i-Si angles of O_i and O_{2i} as a function of the lattice parameter. Open circles represent the results for O_i and diamonds for the staggered O_{2i}. The changes in the lattice constant are calculated from the defect-free bulk lattice constant of 5.39 Å. (b) The Si-O_i-Si angle of O_i as a function of supercell size. Triangles show the results obtained from the cluster calculations, squares the results from the supercell calculations by other authors (Table III), and open circles joined with line the results from our supercell calculations. Supercell or cluster size is given in terms of the number of Si atoms. The defect-free bulk lattice constant of 5.39 Å is used in our calculations.

TABLE IV. Structures of O_{2i}. PP, SC, and C denote the pseudopotential method, supercell and (*H*-terminated) cluster, respectively. The number after SC or C gives the number of Si atoms. The Γ point **k** sampling is used in calculating with the SC of 128 Si atoms. S and SK in parentheses denote the staggered and the skewed O_i-Si-Si-O_i configuration, respectively. In the configuration reported by Ewels *et al.* the oxygen atoms have a common silicon atom. The values without parentheses are pressure-free whereas those in parentheses are calculated with the lattice constant of 5.39 Å of a defect-free bulk silicon.

	Method	Si-$O_{\{1,2\}}$-Si angle	$Si_{\{1,2\}}$-O_1 (Å)	$Si_{\{2,3\}}$-O_2 (Å)	$Si_{\{3,4\}}$-O_2 (Å)
This work	PP SC 128 (S)	(131,126)	(1.65,1.63)	(1.64,1.67)	
	PP SC 128 (SK)	(153,152)	(1.63,1.63)		(1.63,1.63)
	PP SC 32 (S)	136,130 (131,126)	1.65,1.63 (1.65,1.63)	1.63,1.67 (1.63,1.67)	
	PP SC 32 (SK)	157,154 (151,144)	1.62,1.62 (1.63,1.62)		1.63,1.62 (1.63,1.63)
Öberg *et al.*[a]	PP C 42 (SK)	166	1.62,1.64; 1.62,1.65		
Ewels *et al.*[b]	PP C ~60	170	1.52,1.67		

[a]Reference 44.
[b]Reference 48.

crease to 154° (Table III). The value of 154° agrees closely with the experimental one of 162° (Table III). The calculated values in Table III range from 140 ° to 180° our value being on the smaller side. Our calculated Si-O_i bond length of 1.63 Å agrees closely with most of the other calculated ones in Table III.

The calculated structures of O_{2i} are given in Table IV together with previous theoretical studies.[44,48] The oxygen atoms of the staggered O_{2i} [Fig. 1(b)] form a chain along one of the ⟨110⟩ directions. The calculated behavior of the Si-O_i-Si angles as a function of lattice constant is shown in Fig. 3(a). At high pressure both angles are slightly above the value of 120° and similarly to the case of O_i they open when pressure is decreased. However, increasing the size of the supercell does not increase the Si-O_i-Si angles (Table IV). The reason for this is not clear to us but may be due to an insufficient number of silicon atoms to allow a proper relaxation around O_{2i} (or/and the residual O_{2i}-O_{2i} interactions). The symmetric structure where both oxygen atoms would protrude similar to the Si_1-O_1-Si_2 structure in Fig. 1(b) is not stable and relaxes to staggered structure.

For the skewed O_i-Si-Si-O_i structure [Fig. 1(c)] we find that the two angles open and approach each other when either pressure is relieved or when the size of the supercell is increased to 128 atom sites (Table IV). As expected, the Si-O_i-Si angles in this structure consisting of the weakly interacting O_i's are about the same as the corresponding angle of a single O_i (Table III).

2. Vacancy-oxygen complexes

The calculated structures of the vacancy-oxygen complexes are shown in Fig. 4. In *V*O [Fig. 4(a)] the oxygen atom moves from the substitutional (vacancy) site to the [100] direction and forms bonds with the silicon atoms Si_1 and Si_2. The silicon atoms Si_3 and Si_4 form a weak bond that plays a central role in the appearance of the deep levels in the forbidden energy gap. In VO_2 [Fig. 4(b)] both oxygen atoms form symmetrically similar bonds to two silicon atoms as O in *V*O. In V_2O [Fig. 4(c)] the oxygen atom forms bonds with the silicon atoms Si_1 and Si_2 at one end of V_2. The silicon atoms Si_3 and Si_4 form a weak bond in the other end of V_2.

The calculated formation energies and ionization levels of the vacancy-oxygen complexes are listed in Table V together with experiments.[56–58] The dependence of the formation energy on the supercell size was studied calculating the neutral *V*O with three different supercells. The formation energies obtained were found to converge already with the supercell size of 32 atom sites. The formation energies obtained are 2.8, 3.6, and 3.7 eV for the 16, 32, and 64 atom-site supercells, respectively. Also the ionization levels stayed at approximately the same positions when the 32 atom-site supercell was grown to the larger 64 atom-site supercell. Using Γ-point and 128 atom-site supercell leads to a formation energy of 2.7 eV. The lower value is consistent with the previous studies for *V* and V_2 in silicon.[31,32]

A defect having an ionization level 0.16 eV below the conduction band minimum was observed for the first time in the electric measurements by Wertheim[59,60] and Hill[61] although the structure and constituents of the defect were not clear by then. The EPR measurements by Watkins *et al.* revealed that this defect was *V*O (named the *A* center).[56,57] The

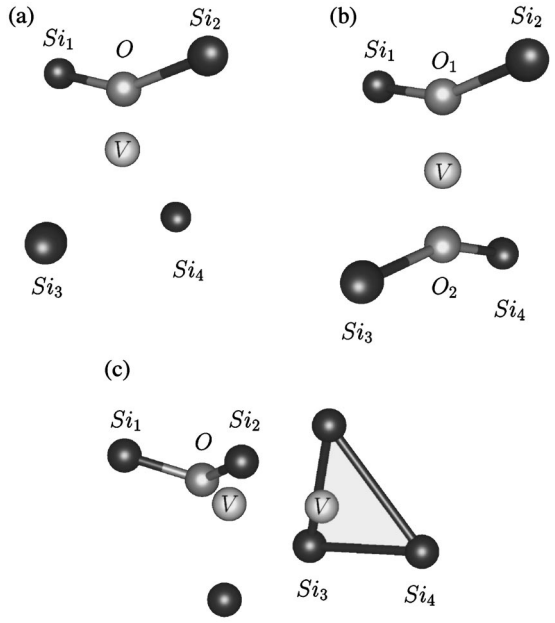

FIG. 4. The calculated structures of the vacancy-oxygen complexes studied: (a) *V*O, (b) VO_2, (c) V_2O. Dark spheres represent silicon atoms, light gray spheres oxygen atoms, and white spheres the positions of the vacancies (*V*).

TABLE V. Calculated formation energies E_f and ionization levels (eV) of the vacancy-oxygen complexes. *V* denotes vacancy. The second column gives the number of silicon atoms in the supercell.

	No. Si atoms	This work	Experiments
*V*O			
E_f	63	3.7	
$(-/0)$	63	0.40	1.0[a]
$(2-/-)$	63	0.53	
trivalent	31	3.9	
VO_2			
E_f	31	3.7	
V_2O			
E_f	62	5.5	
$(-/0)$	62	0.34	0.87[b]
$(2-/-)$	62	0.39	
V_2O_2			
E_f	62	5.6	

[a]References 56,57.
[b]Reference 58.

point symmetry group is C_{2v} and the oxygen atom is attached to the dangling bonds of two silicon atoms of the vacancy [Fig. 4(a)]. Our calculations show that the uppermost occupied state has a node in the mirror plane and is thus an antibonding orbital of type a_1. The experimental ionization level $(-/0)$ of *V*O lies at $E_c-0.17\pm0.01$.[56,57] Figure 5 shows the calculated formation energy plot for *V*O. The ionization levels shown in Fig. 5 are obtained from the total energy using Eqs. (2.2)–(2.4). The calculated ionization levels $(-/0)$ and $(2-/-)$ of *V*O are at 0.40 and 0.53 eV, respectively. The calculated $(-/0)$ level lies about 0.6 eV below the experimental one. For comparison, we find for V_2 from the most accurate calculations (Γ point, 216 atom-site supercell) that the two lowest ionization levels $(0/+)$ and $(-/0)$ lie about 0.2 eV below the corresponding experimental

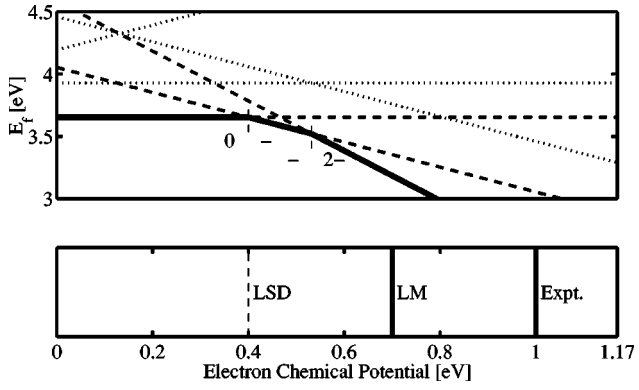

FIG. 5. Formation energy plot for *V*O. The thick line in the upper panel indicates the charge state with the lowest energy. The dashed and dotted lines in the upper panel are the formation energies for the divalently and trivalently bonded oxygen, respectively. The lower panel shows the positions of the $(-/0)$ ionization levels. The experimental value is from Refs. 56 and 57.

levels at 0.25 and $\sim$0.55 eV.[32] The calculated uppermost $(2-/-)$ level for V_2 lies (increasingly) 0.3 eV below the experimental level at 0.75 eV. And, the result that the calculated $(-/0)$ level for *V*O lies 0.6 eV below the experimental level at 1.0 eV close to E_c ($E_c-0.17$ eV) is in line with our results for V_2. It is also clear that the calculated $(2-/-)$ level at 0.53 eV for *V*O could in reality be a resonance state in the conduction band. In any case, the LD approximation in the DFT appears to describe the ionization levels in the upper part of the gap insufficiently analogously with the underestimation of the band gap. This deficiency can be at least partially removed using the LM approximation for valence electrons.[22] Our preliminary LM results for *V*O show that the $(-/0)$ ionization level rises about 0.3 eV towards the experimental value (see the lower panel of Fig. 5). This effect has also been found in the vacancy-substitutional arsenic pair in silicon. The deep level rises from 0.25 to 0.55 eV,[62] while the experimental value for the level is 0.7 eV.

The substitutional oxygen in silicon has also another C_{3v} symmetric structure with a trivalently bonded oxygen. The positive charge states of the divalently bonded C_{2v}-symmetric *V*O are not thermodynamically stable at any value of the electron chemical potential (Fig. 5). This holds also for the trivalently bonded *V*O. The calculated trivalently bonded *V*O structure has a total energy that is 0.3 eV higher in the neutral charge state than the total energy of the C_{2v}-symmetric structure (see Fig 5). For this difference Chadi obtained a value of 0.5 eV.[18] The result by Van Oosten *et al.*[63] that the C_{3v}-symmetric structure has a stable positive charge state could thus not be verified by our calculations.

The formation energy of V_2O is rather high, equal to 5.5 eV (Table V). According to our calculations the energy difference between the high spin state ($S=1$) and the spin compensated state ($S=0$) of the neutral V_2O is only 0.18 eV in favor of the spin compensated case. Thus, thermal excitation to the metastable $S=1$ state is needed before V_2O can be detected in EPR experiments. Our result agrees with the analysis given by Lee and Corbett.[64] Similarly to *V*O also V_2O has two ionization levels in the gap (see Fig. 5). The calculated $(-/0)$ and $(2-/-)$ ionization levels for V_2O are at 0.34 and 0.39 eV, respectively (Table V). Kimerling[58] gives tentatively a value of 0.87 eV ($E_c-0.3$ eV) for the experimental ionization level. The calculated $(-/0)$ level of 0.34 eV lies about 0.5 eV below the experimental one similarly to the case of *V*O.

Table VI lists the calculated binding energies for the vacancy-oxygen complexes. The values are obtained using the most well-converged values available for the formation energies. This approach can lead to small errors due to the dependence of the formation energy on the **k**-point sampling and supercell size.[31]

The pathways for the dissociation of the vacancy-oxygen complexes can be estimated using the binding energies of Table VI. The optimal pathway for the dissociation of VO_2 is

$$VO_2 \overset{1.0\text{ eV}}{\rightarrow} VO+O_i \overset{0.6\text{ eV}}{\rightarrow} V+2O_i\,. \tag{3.1}$$

For V_2O_2 the optimal pathway is

TABLE VI. Calculated binding energies E_b of the vacancy-oxygen complexes. The most well-converged values for the formation energies available have been used: 3.31 and 4.94 eV for the vacancy (V) (Ref. 31) and the divacancy (V_2) (Ref. 32) are from a 216 atom-site supercell calculation with the Γ point Brillouin zone sampling. The formation energies of O_i and O_{2i} are from a 128 atom-site supercell calculation with the Γ point (see Table I).

Row	Constituents	→	Outcome				E_b (eV)
1	$V+O_i$	→	VO				0.8
2	$V+O_{2i}$	→		VO_2			1.6
3	V_2+O_i	→			V_2O		0.5
4	V_2+O_{2i}	→				V_2O_2	1.4
5	$VO+O_i$	→		VO_2			1.0
6	$VO+O_{2i}$	→		VO_2		$+ O_i$	0.8
7	$VO+V$	→			V_2O		1.4
8	$VO+VO$	→				V_2O_2	1.7
9	$VO+Si_i$	→				O_i	6.8
10	VO_2+V	→				V_2O_2	1.4
11	VO_2+Si_i	→				O_{2i}	5.9
12	V_2O+O_i	→				V_2O_2	0.5
13	V_2O+Si_i	→	VO				6.1

$$V_2O_2 \xrightarrow{0.5\ \text{eV}} V_2O+O_i \xrightarrow{0.5\ \text{eV}} V_2+2O_i\,. \tag{3.2}$$

Both pathways lead to increase of O_i content in the crystal.

VO is known to anneal at elevated temperatures.[19,65] The diffusion barrier for VO has been estimated to be low, only 1.84 eV by means of the classical Jiang-Brown potential.[66] Thus, VO can diffuse quite easily to O_i and form VO_2, or two VO's can encounter and form V_2O_2 (Table VI, rows 5 and 8). The energy gain in the former process is approximately the size of the formation energy of O_i (1.1 eV, Table I), because the formation energy of VO_2 is very near that for VO. V_2O_2 may in principle dissociate to VO_2 and V but this is not energetically very favorable (Table VI, row 10).

If O_{2i} is a FDS then it is also reasonable to consider the process where it encounters VO. The result of this process, VO_3, can further dissociate into VO_2 and O_i leading to a net energy gain of 0.8 eV (Table VI, row 6). VO_2 can also be formed from V and O_{2i} (Table VI, row 2). In fact this way is by 0.6 eV more favorable than the formation from VO and O_i (Table VI, rows 2 and 5). V_2O can be formed from O_i and V_2 (Table VI, row 3) or by 0.9 eV more favorably from V and VO (Table VI, row 7).

The formation energy of the silicon self-interstitial (Si_i) when the Fermi level is in the midgap is according to Ref. 67 $\sim$4.2 eV. The process where Si_i encounters a vacancy-oxygen complex always leads to a high energy gain (Table VI rows 9, 11, and 13).

We consider next the structures of the vacancy-oxygen complexes in Fig. 4 in more detail. The calculated structures of the vacancy-oxygen complexes are listed in Table VII together with previous theoretical studies[13,17,18,45,63,68–70] and experiments.[71] According to our calculations in the neutral charge state of VO the oxygen atom is shifted to an [100] direction from the substitutional site such that the Si-O-Si angle is 148° [see Fig. 4(a) and Table VII]. The energy gain when moving from the unrelaxed configuration with the T_d symmetry to the C_{2v} symmetry is 1.3 eV. The energy gain is of the order of 0.6 eV when the T_d-symmetric structure is allowed to relax while keeping the symmetry.

As the number of electrons localized in VO increases the Si-O-Si angle opens and the oxygen atom shifts further in the [100] direction. Our value of 152° of the Si-O-Si angle of VO^- agrees closely with the experimental value of 155° (Table VII).[71] In the negative charge states the extra electron is localized to the weak Si_3-Si_4 bond opposite to the oxygen atom [Fig. 4(a)]. Our results for VO agree closely with the other computational results in Table VII.

The structure of VO_2 resembles the structure of VO. Each of the two oxygen atoms is bonded to two silicon atoms of the vacancy and the Si-O-Si angle of 155° is close to the corresponding value of VO [see Figs. 4(a) and 4(b), Table VII]. Oxygen atoms are repulsed from the vacancy so that the V-$O_{\{1,2\}}$ distance is increased by 0.21 Å from the V-O distance of VO. The O_1-O_2 distance equals 2.45 Å that is in close agreement with the previous computational values (Table VII).

Our results for the structure of V_2O agree closely with the results by Ewels *et al.*[17] (Table VII). Their bond lengths are consistently larger than our values but in contrast to VO the Si-O-Si angle is now larger. Adding electrons to V_2O enhances mainly the Si_3-Si_4 bond (the Si_3-Si_4 distance decreases) and also opens the Si-O-Si angle (Table VII).

B. Local vibrations

1. Interstitial oxygen

There are three experimentally known fundamental low-temperature LV's for O_i which are located at 1136, 517, and 29 cm^{-1}.[6,43,72–75] These LV's may be interpreted using two different models. The traditional model is a puckered Si_2O molecule (symmetry group C_{2v}) according to which the 1136, 517, and 29 cm^{-1} LV's are an asymmetric stretching (B_1), a symmetric stretching (A_1), and a bend (A_1) mode, respectively[6,76] (see also, Refs. 43,73) A difficulty with this model is the fact that experimentally the LV frequency of 517 cm^{-1} does not shift when $^{16}O_i$ is substituted by the $^{18}O_i$ isotope[74] whereas according to the model O_i vibrates and an isotopic shift should be observable. On the other hand, the puckered Si_2O-molecule model does describe correctly the observed large isotopic shift of 52 cm^{-1} in the 1136 cm^{-1} LV frequency.[74] The above symmetry classification neglects the silicon crystal around the Si_2O molecule. When the cystalline environment is taken into account the symmetry group of the puckered Si_2O molecule is C_2 and the 1136, 517, and 29 cm^{-1} LV's have the B, A, and A representations, respectively.

A second more recent model is a linear Si_2O molecule (symmetry group D_{3d}) based on a low (1 meV) BC energy and the associated quantum delocalization of O_i such that its probability distribution is centered at the BC.[50,77–79] According to this model the 1136 and 517 cm^{-1} LV's are an asymmetric stretching (A_{2u}) mode and a transverse silicon mode induced by a nonmoving O_i (E_u), respectively.[50] In addition, the model gives an IR inactive symmetric stretching mode (A_{1g}) at 596 cm^{-1}.[50]

TABLE VII. Structures of the vacancy-oxygen complexes in different charge states. Distances are given in Å. The $2\times2\times2$ MP Brillouin zone sampling is used in this work. The methods included are the pseudopotential (PP), Hartree-Fock (HF), scattered-wave (SW) X_α, semiempirical (MNDO), and Green matrix (G) method. SC and C denote supercell and (*H*-terminated) cluster, respectively. The number after SC or C gives the number of Si atoms.

	Method	O-Si$_{\{1,2\}}$	Si-O-Si angle (deg.)	*V*-O	O_1-O_2	Si_3-Si_4	Symmetry
VO^0							
This work	PP SC 63	1.69	148	1.01		3.16	C_{2v}
Ewels *et al.*[a]	PP C ~70	1.754	138	0.934		3.77	
Van Oosten *et al.*[b]	HF C 4,10			0.95			
Snyder and Corbett[c]	HF C 4			1.04			
Hjalmarson and Jennison[d]	HF C 4			1.1			
DeLeo *et al.*[e]	SWX_α, MNDO C 4			1.0			
VO^-							
This work	PP SC 63	1.68	152	1.05		3.37	C_{2v}
Experiment[f]			155				
VO^{2-}							
This work	PP SC 63	1.67	158	1.12		3.36	C_{2v}
VO_2							
This work	PP SC 31	1.70	155	1.22	2.45	3.26	D_{2d}
Ewels *et al.*[a]	PP C ~70	1.710	147		2.61		D_{2d}
Chadi[g]	PP SC 31				2.5		
Kelly[h]	G				2.6		
Snyder and Corbett[c]	HF C 4				2.44		D_{2d}
DeLeo *et al.*[i]	SWX_α, MNDO C 4				2.5		
V_2O^0							
This work	PP SC 62	1.68	138	0.78,2.90		3.04	C_{1h}
Ewels *et al.*[a]	PP C ~70	1.73,1.72	143				
V_2O^-							
This work	PP SC 62	1.69	142	0.85,2.90		3.01	C_{1h}
V_2O^{2-}							
This work	PP SC 62	1.70	148	0.97,2.90		2.93	C_{1h}

[a]Reference 17.
[b]Reference 63.
[c]Reference 13.
[d]Reference 68.
[e]Reference 69.
[f]Reference 71.
[g]Reference 18.
[h]Reference 45.
[i]Reference 70.

We have calculated the LV's of O_i both using the relaxed lattice constant $a=5.43$ Å ($P=0$ kbar) and the lattice constant $a=5.39$ Å of defect-free bulk silicon ($P=16$ kbar). The calculated LV modes are shown in Fig. 6 and the calculated LV frequencies are listed in Table VIII together with other calculations[16,46,51,80] and experiments.[43,74,75,81]

The calculated asymmetric stretching frequency of 1098 cm^{-1} and its isotopic shifts agree closely with the experimental values and with the calculations by Jones *et al.*[51] The calculated isotopic shifts agree also closely with those reported by Snyder *et al.*[80] The calculated direction of the transition dipole which is parallel to the [111] direction also agrees with the experiments.[6]

The calculated symmetric stretching frequency of 630 cm^{-1} lies 113 cm^{-1} above the second experimental frequency of 517 cm^{-1} and the calculated isotopic shift of 2 cm^{-1}—though small—differs from the strict experimental value of 0 cm^{-1}. The direction of the transition dipole—perpendicular to the [111] direction—agrees with the experiments.[76] The calculated results for the symmetric stretching frequency thus agree moderately well with the experimental data. And in any case, the calculated symmetric stretching mode at 630 cm^{-1} is the *only local* mode of O_i that could be associated with the experimental frequency of 517 cm^{-1}. The calculated modes starting from the next highest frequency of 544 cm^{-1} are *all* delocalized.[82] However, our analysis for O_{2i} below shows that the experimental LV frequency of 517 cm^{-1} is in fact *not* to be associated with the symmetric stretching mode at 630 cm^{-1} but with a localized oxygen induced Si mode because the symmetric

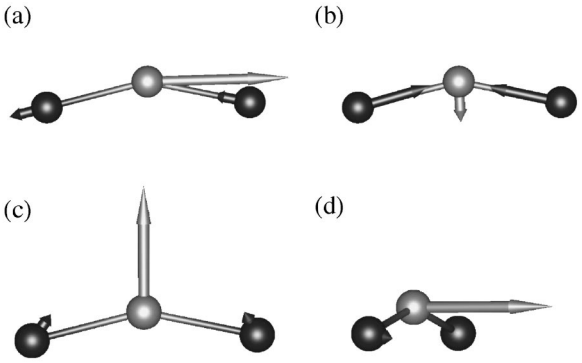

FIG. 6. Local vibrational modes of O_i. (a) 1098 cm^{-1}, (b) 630 cm^{-1}, (c) 158 cm^{-1}, and (d) 130 cm^{-1}. Notice the rotated view in (d). Dark spheres represent silicon atoms, light gray spheres oxygen atoms. The vibration amplitudes of the atoms not shown are negligible.

stretching modes of the skewed O_i-Si-Si-O_i configuration are not detected experimentally but the weak interaction between the two O_i's is capable of forming a localized oxygen induced Si mode at 558 cm^{-1}, about 9 cm^{-1} above the region of the delocalized modes. This interpretation parallels the characterization of the 517 cm^{-1} mode by Artacho *et al.*[50] According to Artacho *et al.* the symmetric stretching LV is not seen in the experiments because this mode is IR inactive for a linear Si_2O molecule. Although the symmetric stretching LV of the puckered Si_2O molecule obtained [Fig. 6(b)] is IR active and could in principle be seen in experiments the small amplitude of O_i makes this probably impossible in practice. One way to find out the nature of the 517 cm^{-1} mode is to measure the isotopic shifts when one (both) of the Si atoms neighboring O_i is (are) replaced by the ^{29}Si isotope. The corresponding calculated isotopic shifts in the symmetric stretching 630 cm^{-1} LV mode are 5 and 10 cm^{-1} (Table VIII) implying that these isotopic shifts should be discernible in the 517 cm^{-1} mode if present.[83] However, to the best of the knowledge of the present authors the experimental shifts in the 517 cm^{-1} mode have not been reported.

Below the delocalized modes we find two LV modes that have the lowest of all the frequencies: the bend mode at 158 cm^{-1} and the mode consisting of the vibration around the [111] axis at 130 cm^{-1} [Figs. 6(c) and 6(d), respectively]. The bend mode is the lowest of the three modes of the puckered (planar) Si_2O-molecule model. However, due to the crystalline environment the mode consisting of the vibration around the [111] axis becomes the lowest LV mode. Quantitatively, the calculated frequencies of 158 and 130 cm^{-1} as well as their isotopic shifts (5 cm^{-1} each) are larger than the experimental frequency of 29 cm^{-1} and its isotopic shift of 2 cm^{-1} (Table VIII). Usually the far IR spectrum of O_i is explained with a quantum model of a linear Si_2O molecule where the oxygen atom moves in a central field in a plane perpendicular to the [111] axis.[43,50,77–79] This type of very refined comparison is beyond the accuracy of the present method. However, we consider next the BC energy which is a decisive factor in this quantum model. The BC energy was investigated by restricting the oxygen atom to lie in the center of the coordinates of the two bonding silicon atoms but otherwise allowing all the atoms to fully relax. The calculated results are given in Table IX together with other calculations. Our and Chadi's[18] DFT LD PP calculations give significant BC energies of 20 and 100 meV,

TABLE VIII. Local vibration frequencies (cm^{-1}) of O_i. The methods included are the pseudopotential (PP) and semiempirical (MINDO/3) method. SC, C, and CC denote supercell, (*H*-terminated) cluster, and cyclic cluster, respectively. The number after SC, C, or CC gives the corresponding number of Si atoms. The values calculated using the lattice constant of 5.390 Å of defect-free bulk silicon corresponding to a pressure of 16 kbar are given in the third column in parentheses. The numbers in parentheses in the last four columns are the isotopic shifts downwards (cm^{-1}). $^{16}O_i^{28}Si$ denotes the case where all Si atoms are of the ^{28}Si isotope. $^{28}Si^{16}O_i^{29}Si$ denotes the case where one of the Si atoms neighboring O_i is changed into a ^{29}Si isotope. In the calculations by Snyder *et al.* only O_i and its two nearest neighbor Si atoms are moving. The experimental values are measured at low temperatures $\leqslant 6$ K.

	Method	$^{16}O_i^{28}Si$	$^{18}O_i^{28}Si$	$^{28}Si^{16}O_i^{29}Si$	$^{29}Si^{16}O_i^{29}Si$	$^{16}O_i^{30}Si$
This work	PP SC 32	1098(1083)	1048(50)	1097(1)	1094(4)	1090(8)
		630(617)	628(2)	626(5)	621(10)	610(20)
		158(128)	153(5)	158(0)	158(0)	155(3)
		130(102)	125(5)	130(0)	130(0)	128(2)
Jones *et al.*[a]	PP C 44	1104	1051(53)			1098(6)
		554	553(1)			534(20)
Deák *et al.*[b]	MINDO/3 CC 32	1248				
Snyder *et al.*[c]	MINDO/3 C 8	1275		1273(2)	1271(4)	1267(8)
		699		693(6)	687(12)	675(24)
Saito and Oshiyama[d]	PP C 10	1187				
Experiments		1136[e,f]	1084(52)[e,f]	1134(2)[g]		1129(7)[g]
		517[e,f]	517(0)[e,f]			
		29[f,h]	27(2)[f,h]			

[a]Reference 51.
[b]Reference 16.
[c]Reference 80.
[d]Reference 46.
[e]Reference 74.
[f]Reference 43.
[g]Reference 81.
[h]Reference 75.

TABLE IX. The bond center energy of O_i with respect to the absolute minimum (meV). The methods included are the pseudopotential (PP), Hartree-Fock (HF), and semiempirical (MINDO/3) method. SC, C, and CC denote supercell, (*H*-terminated) cluster, and cyclic cluster, respectively. The number after SC, C, or CC gives the number of Si atoms. The value in parentheses is calculated using the lattice constant of 5.390 Å of bulk silicon corresponding to a pressure of 16 kbar.

	Method	
This work	PP SC 128 (Γ)	20
	PP SC 32	20(39)
Chadi[a]	PP SC 32	~100
Artacho *et al.*[b]	HF C 8	1
Deák *et al.*[c]	MINDO/3 CC 32	0

[a]Reference 18.
[b]Reference 50.
[c]Reference 16.

respectively, whereas the Hartree-Fock method[50] and the semiempirical MINDO/3 method[16] have a tendency to give vanishing BC energies. Since the calculated LV frequencies are larger than the experimental value of 29 cm^{-1} our BC energy in Table IX seems to be somewhat overestimated. However, it is difficult to infer from the present calculation whether the BC energy would in reality diminish to the extent that O_i becomes quantum delocalized as is required by the linear Si_2O-molecule model.

The pressure coefficients and Grüneisen parameters ($\gamma = -\partial \ln \omega / \partial \ln V$)[38] for the LV frequencies can be calculated from the values given in Table VIII. Assuming a linear pressure dependence we get the pressure coefficients and the Grüneisen parameters listed in Table X. All pressure coefficients as well as the Grüneisen parameters are negative. This behavior is common in tetrahedrally coordinated systems and is consistent with the fact that the average overall Grüneisen parameter of bulk silicon crystal is negative at low temperatures. The first pressure coefficient agrees reasonably well with the corresponding experimental value of about -0.3 cm^{-1}/kbar.[55]

2. Interstitial oxygen pair

When two O_i's approach each other to form O_{2i} in a staggered or skewed O_i-Si-Si-O_i configuration [see Figs. 1(b) and 1(c)] the mutual interactions between the O_i's cause splittings and shifts in the LV frequencies of O_i.[84] This behavior is displayed in Fig. 7 showing clearly the larger splittings for the staggered configuration due to the stronger O_i-O_i interactions in this case.[10,44,74,85] Mutual interactions between the two O_i's cause the formation of new *local* oxygen induced Si modes around 560 cm^{-1}—shown for the skewed O_i-Si-Si-O_i configuration in Fig. 8. Consequently, relatively distantly spaced and thus weakly interacting O_i's are capable of forming a localized mode that in this case is 9 cm^{-1} above the region of the delocalized modes. A comparison in Fig. 7 completed with a comparison of isotopic shifts[84] shows that the four experimental frequencies at 1060, 1012, 690, and 556 cm^{-1} belonging to one configuration of O_{2i} (the solid bars in the lowest row in Fig. 7)[10,44,85] originate from the staggered O_{2i}. The experimental frequency at 1105 cm^{-1} from a different configuration of O_{2i} (the dash-dotted bar in Fig. 7)[10] originates then from the skewed O_i-Si-Si-O_i configuration.[84]

By comparing the O_i panel with the O_{2i} panel in Fig. 7 it is immediately obvious that the calculated symmetric stretch-

TABLE X. Pressure coefficients and Grüneisen parameters γ for the local vibration frequencies of O_i.

	Frequency (cm^{-1})	Pressure coefficient (cm^{-1}/kbar)	γ
This work	1098	−0.93	−0.64
	630	−0.80	−0.96
	158	−1.85	−8.85
	130	−1.73	−10.04
Experiments	1136[a,b]	~−0.3[c]	

[a]Reference 74.
[b]Reference 43.
[c]Reference 55.

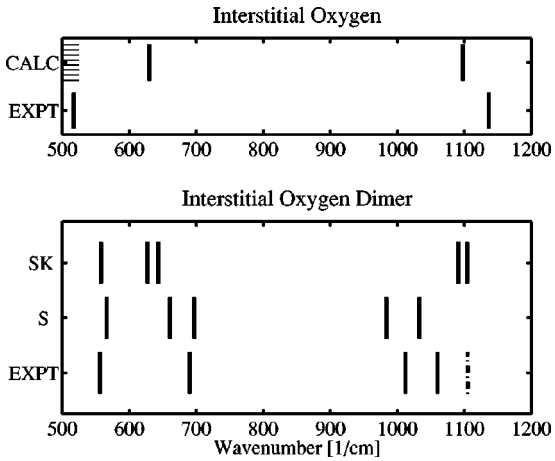

FIG. 7. Local vibration frequencies for O_i and O_{2i}. CALC, EXPT, SK, and S denote our calculations, experiments from Refs. 10,44,74,85, (calculated) skewed O_i-Si-Si-O_i and staggered configurations, respectively. Stripes in the upper panel represent the region of delocalized vibration modes. The experimental dash-dotted bar in the lower panel belongs to a different configuration than the solid bars.

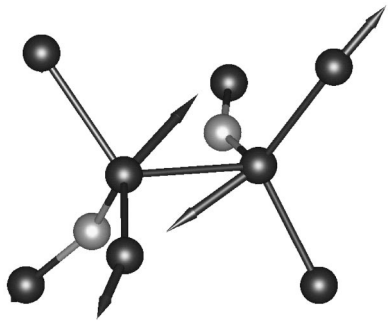

FIG. 8. Oxygen induced silicon mode of the skewed O_i-Si-Si-O_i configuration of O_{2i} at 558 cm^{-1}. Dark spheres represent silicon atoms, light gray spheres oxygen atoms. The vibration amplitudes of the atoms not shown are negligible.

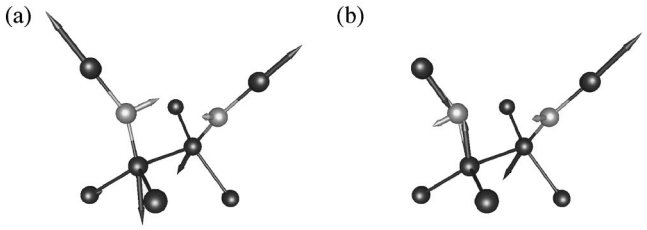

FIG. 9. Symmetric stretching modes of the skewed O_i-Si-Si-O_i configuration of O_{2i}: (a) 643 cm^{-1}, (b) 627 cm^{-1}. Dark spheres represent silicon atoms, light gray spheres oxygen atoms. The vibration amplitudes of the atoms not shown are negligible.

ing mode of O_i at 630 cm^{-1} cannot be related to the experimental mode at 517 cm^{-1}. Instead, this mode is most probably related to a localized oxygen induced Si mode of O_{2i}. The symmetric stretching mode of O_i is not detected experimentally because either a linear Si_2O molecule is IR inactive[50] or in our case of the puckered Si_2O molecule the amplitude of O_i [see Fig. 6(b)] is too small. For the same reason both symmetric stretching modes of the skewed O_i-Si-Si-O_i configuration—shown in Fig. 9—as well as the lower frequency of the symmetric stretching frequency pair of the staggered O_{2i} are not discernible in the IR absorption experiments[84]).

The calculated pressure dependencies of the LV frequencies of O_{2i} are listed in Table XI. Assuming a linear pressure dependence we get the pressure coefficients and the Grüneisen parameters also listed in Table XI. To the best of the authors' knowledge no experimental pressure coefficients or Grüneisen parameters exist for O_{2i} for comparison. It is interesting to observe the following trend. The pressure coefficients and the Grüneisen parameters γ of the symmetric stretching mode increase from negative to positive values when proceeding from O_i (Table X) to the skewed O_i-Si-Si-O_i configuration of O_{2i} to the staggered configuration of O_{2i} (Table XI) (i.e., the mutual interaction of the two O_i's increases). On the other hand, no similar clear trend is seen in the asymmetric stretching case.

3. Vacancy-oxygen complexes

Since an oxygen atom in *V*O (*A* center) forms strong bonds with two silicon atoms passivating their dangling bonds (Fig. 4, Table VII) the LV modes of *V*O resemble those of O_i: an asymmetric stretching mode at a higher frequency and a symmetric stretching mode at a lower frequency. In VO_2 each of the two oxygen atoms forms strong bonds with two silicon atoms and accordingly all four dangling bonds are passivated. The LV's of VO_2 thus consist basically of the LV's of two separate *V*O's modified by the interactions between the oxygen atoms. In the case of V_2O the oxygen atom forms strong bonds with two silicon atoms at one end of V_2 passivating two of the six dangling bonds available in V_2 altogether. Again the LV's of V_2O resemble those of *V*O.

The calculated LV frequencies for *V*O, VO_2, and V_2O together with other calculations[16,17,63,70] and experiments[86–89] are listed in Table XII. Consider first *V*O (symmetry goup C_{2v}). The calculated LV modes of *V*O are shown in Fig. 10. The calculated frequency of the asymmetric stretching mode (B_1) of 843 cm^{-1} agrees closely with the experimental value of 835 cm^{-1} but there are large differences ($\sim$200 cm^{-1}) between the different calculations. According to our calculations the addition of electrons to *V*O increases the LV frequency of the asymmetric stretching mode which is also observed experimentally (Table XII). However, the experimentally observed increase (50 cm^{-1}) is much stronger than the calculated increase (7 cm^{-1}). The reason for this difference is not clear to us. On the other hand, when ^{16}O is replaced by ^{18}O our calculations give for the isotopic shift in the same asymmetric stretching mode exactly the experimental value of 37 cm^{-1}. The calculated symmetric stretching mode (A_1) at 540 cm^{-1}—though in principle IR active—has not been detected experimentally. In this mode the amplitude of the oxygen atom is small as is also the isotopic shift.

To check the results obtained solving the eigenvalue problem of the dynamical matrix we performed also a direct molecular dynamics simulation for *V*O in a neutral charge state. The peaks of the LV modes in the phonon spectrum are obtained from the power spectrum, i.e., from the real part of the Fourier transform of the velocity autocorrelation function [Eq. (2.8)]. The obtained power spectrum is shown in Fig. 11 together with the vibration density of states obtained using the dynamic matrix. The power spectrum gives practically the same LV frequency peaks as the diagonalization of the dynamic matrix (about 850 and 540 cm^{-1}).

When a second oxygen atom is bonded to the two remaining dangling bonds in *V*O to form VO_2 one would intuitively expect that the LV frequencies approach those of O_i. Our calculations indeed show this general tendency that is also observed experimentally (Tables XII and VIII). The symmetry group of VO_2 is D_{2d}. The calculated, essentially degenerate, LV modes (*E*) of the highest frequency of 912 cm^{-1} (see Table XII) are shown in Figs. 12(a) and 12(b). These modes consist of the asymmetric stretching vibration of one

TABLE XI. Pressure dependence of the local vibration frequencies of O_{2i}. The frequencies in the second and third column are given in cm^{-1}. γ denotes the Grüneisen parameter.

Configuration	0 kbar	31 kbar	Pressure coefficient (cm^{-1}/kbar)	γ
staggered	1033,984	1008,959	−1.04,−1.04	−0.78,−0.82
	697,661	698,664	0.04,0.13	0.05,0.15
	566	559	−0.29	−0.40
skewed O_i-Si-Si-O_i	1104,1091	1068,1032	−1.16,−1.90	−0.91,−1.51
	643,627	635,614	−0.26,−0.42	−0.35,−0.58
	558	544	−0.45	−0.70

TABLE XII. Local vibration frequencies (cm^{-1}) of *V*O (A center), VO_2, and V_2O. The methods included are the pseudopotential (PP), Hartree-Fock (HF), scattered-wave (SW) X_α, and semiempirical (MINDO/3, MNDO) method. SC, C, and CC denote supercell, (*H*-terminated) cluster, and cyclic cluster, respectively. The number after SC, C, or CC gives the number of Si atoms. The isotopic shifts downwards (cm^{-1}) are given in parentheses.

Author/Defect	Method	$V^{16}O$	$V^{16}O^-$	$V^{16}O^{2-}$	$V^{18}O$	$V^{16}O_2$	$V^{18}O_2$	$V_2^{16}O$	$V_2^{18}O$
This work	PP SC 32	843	850	862	806(37)	912	871(41)	829	794(35)
		540	539	536	537(3)	594,554	587(7),551(3)	568	566(2)
Ewels *et al.*[a]	PP C ~70	787			749(38)	807	768(39)	791	753(38)
						656	638(19)		
						574	571(4)		
						564	555(9)		
van Oosten *et al.*[b]	HF C 4,10	899							
		364							
Deák *et al.*[c]	MINDO/3 CC 32	990				995			
DeLeo *et al.*[d]	SWX_α, MNDO C 4	800				847			
Experiments									
		835[e]	885[e]		798(37)[f]	895[g]	850(39)[h]		

[a]Reference 17.
[b]Reference 63.
[c]Reference 16.
[d]Reference 70.
[e]Reference 86, 10 K.
[f]Reference 87, 77 K.
[g]Reference 88, 10 K.
[h]Reference 89, 300 K.

oxygen atom the other oxygen atom being nonmoving. It is obvious that the nonmoving oxygen atom does not ''experience'' the motion of the moving oxygen atom because its amplitude vector points along the Si-Si direction perpendicular to the O-O line. The calculated two LV modes of the symmetric stretching type are shown in Figs. 12(c) and 12(d). In these modes the oxygen atoms move on the O-O line and do interact. As expected, the mode where the oxygen atoms vibrate 180° out of phase (A_1) has a higher frequency (594 cm^{-1}) than the mode where they vibrate in phase (B_2, 554 cm^{-1}). The uppermost calculated frequency (912 cm^{-1}) agrees closely with the experimental one of 895 cm^{-1} (and is slightly higher as expected due to the overbinding of the LD approximation). Also, the calculated isotopic shift of 41 cm^{-1} agrees closely with the experimental value of 39 cm^{-1}. The calculated LV mode at 594 cm^{-1} is IR inactive. The calculated LV mode at 554 cm^{-1} is IR

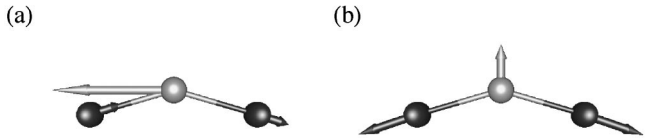

FIG. 10. Local vibration modes for *V*O. (a) 843 cm^{-1} and (b) 540 cm^{-1}. The vibration amplitudes of the atoms not shown are negligible.

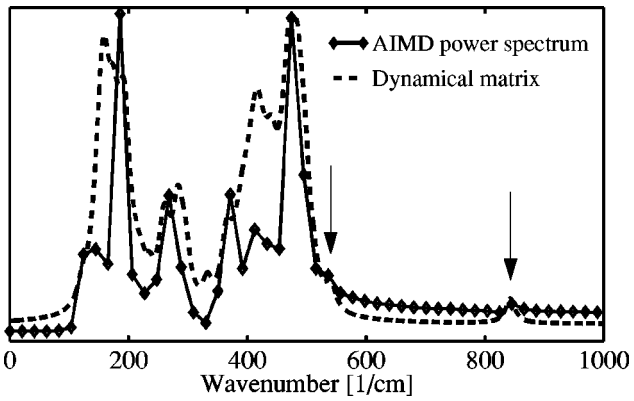

FIG. 11. Power spectrum (diamonds and solid line) and vibration density of states from the dynamic matrix (dashed line) of *V*O in arbitrary units. The molecular dynamics simulation is performed at $T \approx 260$ K.

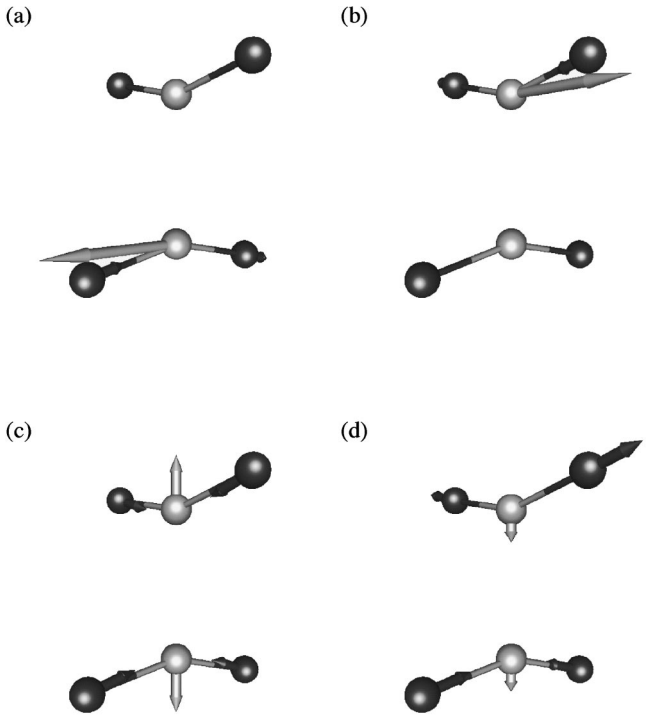

FIG. 12. The local vibration modes of VO_2. (a) 913 cm^{-1}, (b) 911 cm^{-1}, (c) 594 cm^{-1}, and (d) 554 cm^{-1}. The vibration amplitudes of the atoms not shown are negligible.

active and could be observed experimentally though the amplitudes of the oxygen atoms are small as is also the isotopic shift (Table XII). The calculated isotopic shift of the highest mode of 41 cm^{-1} agrees closely with that of 39 cm^{-1} obtained by Ewels *et al.*[17] though there is a large quantitative difference between the LV frequencies (912 vs 807 cm^{-1}).

The calculated LV modes of V_2O are essentially the same as those of VO (Fig. 10). The calculated LV frequency of the asymmetric stretching mode and its isotopic shift (Table XII) agree closely with the results obtained by Ewels *et al.*[17] To the best of our knowledge no experimental frequencies are available for comparison.

IV. CONCLUSIONS

The formation and binding energies, the ionization levels, the structures, and the local vibrations of the charged interstitial oxygen and vacancy-oxygen complexes O_i, O_{2i}, O_{3i}, VO, VO_2, and V_2O in silicon have been studied using a self-consistent density functional theory based total-energy pseudopotential method. The calculated results agree in general closely with available experimental data.

The most prominent new results are as follows. The calculated ionization levels and the associated structures of the various charge states for VO and V_2O as well as the local vibration modes for the negative charge states of VO have been presented. The origin of the basic infrared absorption peaks of O_i and O_{2i} have been explained. The experimental frequencies of O_i at 1136 and 517 cm^{-1} are associated with an asymmetric stretching mode of O_i and an oxygen induced silicon mode of weakly interacting O_i's, respectively. The calculated effects of pressure on the structures and local vibration frequencies (Grüneisen parameters) of O_i and O_{2i} have been presented.

ACKNOWLEDGMENTS

This work has been supported by the Academy of Finland. The authors wish to thank Professor M. Puska, Professor K. Laasonen, and Dr. S. Pöykkö for many valuable discussions. We acknowledge the generous computing resources of the Center for the Scientific Computing (CSC), Espoo, Finland. M. P. and T. M. acknowledge the financial support of the Väisälä Foundation.

*Electronic address: Marko.Pesola@hut.fi
†Electronic address: Juhani.Boehm@hut.fi
‡Electronic address: tomi_mattila@nrel.gov
§Electronic address: Risto.Nieminen@hut.fi

[1] C. S. Fuller, J. A. Ditzenberger, N. B. Hannay, and E. Buehler, Phys. Rev. **96**, 833 (1954).
[2] P. Wagner and J. Hage, Appl. Phys. A: Solids Surf. **49**, 123 (1989).
[3] H. Navarro, J. Griffin, J. Weber, and L. Genzel, Solid State Commun. **58**, 151 (1986).
[4] W. Cazcarra and P. Zunino, J. Appl. Phys. **51**, 4206 (1980).
[5] W. Götz, G. Pensl, and W. Zulehner, Phys. Rev. B **46**, 4312 (1992).
[6] J. W. Corbett, R. S. McDonald, and G. D. Watkins, J. Phys. Chem. Solids **25**, 873 (1964).
[7] J. C. Mikkelsen, in *Oxygen, Carbon, Hydrogen, and Nitrogen in Crystalline Silicon*, MRS Symposia Proceedings No. 59, edited by J. C. Mikkelson, Jr., S. J. Pearton, J. W. Corbett, and P. W. Pennycook (Materials Research Society, Pittsburgh, 1986), p. 19.
[8] P. Wagner, J. Hage, J. M. Trombetta, and G. D. Watkins, Mater. Sci. Forum **83-87**, 401 (1992).
[9] R. C. Newman, in *Early Stages of Oxygen Precipitation in Silicon*, edited by R. Jones (Kluwer Academic, Dordrecht, 1996), p. 19.
[10] L. I. Murin, T. Hallberg, V. P. Markevich, and J. L. Lindström, Phys. Rev. Lett. **80**, 93 (1998).
[11] *Early Stages of Oxygen Precipitation in Silicon* (Ref. 9), and references therein.
[12] *Prooceedings of the 19th International Conference on Defects in Semiconductors*, Aueiro, Portugal, 1997 [Mater. Sci. Forum **258-263** (1997), and references therein].
[13] L. C. Snyder and J. W. Corbett, in *Oxygen, Carbon, Hydrogen and Nitrogen in Crystalline Silicon* (Ref. 7), p. 207.
[14] D. J. Chadi, Phys. Rev. B **41**, 10 595 (1990).
[15] M. Needels, J. D. Joannopoulos, Y. Bar-Yam, and S. T. Pantelides, Phys. Rev. B **43**, 4208 (1991).
[16] P. Deák, L. C. Snyder, and J. W. Corbett, Phys. Rev. B **45**, 11 612 (1992).
[17] C. P. Ewels, R. Jones, and S. Öberg, Mater. Sci. Forum **196-201**, 1297 (1995).
[18] D. J. Chadi, Phys. Rev. Lett. **77**, 861 (1996).
[19] J. W. Corbett, G. D. Watkins, and R. S. McDonald, Phys. Rev. **135**, A1381 (1964).
[20] P. Hohenberg and W. Kohn, Phys. Rev. **136**, B864 (1964).
[21] W. Kohn and L. J. Sham, Phys. Rev. **140**, A1133 (1965).
[22] G. E. Engel and W. E. Pickett, Phys. Rev. B **54**, 8420 (1996).
[23] O. Gunnarsson and B. I. Lundqvist, Phys. Rev. B **13**, 4274 (1976).
[24] J. P. Perdew and A. Zunger, Phys. Rev. B **23**, 5048 (1981).
[25] D. M. Ceperley and B. J. Alder, Phys. Rev. Lett. **45**, 566 (1980).
[26] D. R. Hamann, Phys. Rev. B **40**, 2980 (1989).
[27] L. Kleinman and D. M. Bylander, Phys. Rev. Lett. **48**, 1425 (1982).
[28] D. Vanderbilt, Phys. Rev. B **41**, 7892 (1990); K. Laasonen, A. Pasquarello, R. Car, C. Lee, and D. Vanderbilt, *ibid.* **47**, 10 142 (1993).
[29] N. N. Greenwood and A. Earnshaw, *Chemistry of the Elements* (Pergamon, New York, 1984), p. 720.
[30] H. J. Monkhorst and J. D. Pack, Phys. Rev. B **13**, 5188 (1976).
[31] M. J. Puska, S. Pöykkö, M. Pesola, and R. M. Nieminen, Phys. Rev. B **58**, 1318 (1998).
[32] M. Pesola, J. von Boehm, S. Pöykkö, and R. M. Nieminen, Phys. Rev. B **58**, 1106 (1998).
[33] S. Pöykkö, M. J. Puska, and R. M. Nieminen, Phys. Rev. B **57**, 12 174 (1998).
[34] G.-X. Qian, R. M. Martin, and D. J. Chadi, Phys. Rev. B **38**, 7649 (1988).
[35] S. B. Zhang and J. E. Northrup, Phys. Rev. Lett. **67**, 2339 (1991).
[36] T. Mattila and R. M. Nieminen, Phys. Rev. B **54**, 16 676 (1996).
[37] S. Pöykkö, M. J. Puska, and R. M. Nieminen, Phys. Rev. B **53**, 3813 (1996).
[38] H. Ibach and H. Lüth, *Solid-State Physics* (Springer-Verlag, Berlin, 1995).

[39] Ville Sammalkorpi (private communication).
[40] Th. Köhler, Th. Frauenheim, and G. Jungnickel, Phys. Rev. B **52**, 11 837 (1995).
[41] M. P. Allen and D. J. Tildesley, *Computer Simulation of Liquids* (Clarendon, Oxford, 1987).
[42] R. Virkkunen, K. Laasonen, and R. M. Nieminen, J. Phys.: Condens. Matter **3**, 7455 (1991).
[43] D. R. Bosomworth, W. Hayes, A. R. L. Spray, and G. D. Watkins, Proc. R. Soc. London, Ser. A **317**, 133 (1970).
[44] S. Öberg, C. P. Ewels, R. Jones, T. Hallberg, J. L. Lindström, L. I. Murin, and P. R. Briddon, Phys. Rev. Lett. **81**, 2930 (1998).
[45] P. J. Kelly, Mater. Sci. Forum **38-41**, 269 (1989).
[46] M. Saito and A. Oshiyama, Phys. Rev. B **38**, 10 711 (1988).
[47] L. C. Snyder, J. W. Corbett, P. Deak, and R. Wu, in *Defects in Electronic Materials*, edited by M. Stavola, MRS Symposia Proceedings No. 104 (Materials Research Society, Pittsburgh, 1988), p. 179.
[48] C. P. Ewels, R. Jones, and S. Öberg, in *Early Stages of Oxygen Precipitation in Silicon* (Ref. 9), p. 141.
[49] C. Kittel, *Introduction to Solid State Physics* (Wiley, New York, 1968).
[50] E. Artacho, A. Lizón-Nordström, and F. Ynduráin, Phys. Rev. B **51**, 7862 (1995).
[51] R. Jones, A. Umerski, and S. Öberg, Phys. Rev. B **45**, 11 321 (1992).
[52] P. J. Kelly and R. Car, Phys. Rev. B **45**, 6543 (1992).
[53] S. K. Estreicher, Phys. Rev. B **41**, 9886 (1990).
[54] E. Martinez, J. Plans, and F. Yndurain, Phys. Rev. B **36**, 8043 (1987).
[55] M. D. McCluskey and E. E. Haller, Phys. Rev. B **56**, 9520 (1997).
[56] G. D. Watkins, J. W. Corbett, and R. M. Walker, J. Appl. Phys. **30**, 1198 (1959).
[57] G. D. Watkins and J. W. Corbett, Phys. Rev. **121**, 1001 (1961).
[58] L. C. Kimerling, Inst. Phys. Conf. Ser. **31**, 221 (1977).
[59] G. K. Wertheim, Phys. Rev. **105**, 1730 (1957).
[60] G. K. Wertheim, Phys. Rev. **110**, 1272 (1958).
[61] D. E. Hill, Phys. Rev. **114**, 1414 (1959).
[62] J. Lento, M. Pesola, J.-L. Mozos, and R. M. Nieminen (unpublished).
[63] A. B. van Oosten, A. M. Frens, and J. Schmidt, Phys. Rev. B **50**, 5239 (1994).
[64] Y.-H. Lee and J. W. Corbett, Phys. Rev. B **13**, 2653 (1976).
[65] C. A. Londos, G. I. Georgiou, L. G. Fytros, and K. Papastergiou, Phys. Rev. B **50**, 11 531 (1994).
[66] P. J. Grönberg, J. von Boehm, and R. M. Nieminen, in *Early Stages of Oxygen Precipitation in Silicon* (Ref. 9), p. 441.
[67] J. -L. Mozos and R. M. Nieminen, in *Properties of Crystalline Silicon*, edited by Robert Hull (EMIS, London, 1998), and references therein.
[68] H. P. Hjalmarson and D. R. Jennison, Phys. Rev. B **31**, 1208 (1985).
[69] G. G. DeLeo, W. B. Fowler, and G. D. Watkins, Phys. Rev. B **29**, 3193 (1984).
[70] G. G. DeLeo, C. S. Milsted, Jr., and J. C. Kralik, Phys. Rev. B **31**, 3588 (1985).
[71] T. Gregorkiewicz, H. H. P. Th. Bekman, and C. A. J. Ammerlaan, Phys. Rev. B **38**, 3998 (1988).
[72] W. Kaiser, P. H. Keck, and C. F. Lange, Phys. Rev. **101**, 1264 (1956).
[73] H. J. Hrostowski and R. H. Kaiser, Phys. Rev. **107**, 966 (1957).
[74] H. J. Hrostowski and B. J. Alder, J. Chem. Phys. **33**, 980 (1960).
[75] W. Hayes and D. R. Bosomworth, Phys. Rev. Lett. **23**, 851 (1969).
[76] M. Stavola, Appl. Phys. Lett. **44**, 514 (1984).
[77] H. Yamada-Kaneta, C. Kaneta, and T. Ogawa, Phys. Rev. B **42**, 9650 (1990).
[78] E. Artacho, F. Ynduráin, B. Pajot, R. Ramírez, C. P. Herrero, L. I. Khirunenko, K. M. Itoh, and E. E. Haller, Phys. Rev. B **56**, 3820 (1997).
[79] R. Ramírez, C. P. Herrero, E. Artacho, and F. Ynduráin, J. Phys.: Condens. Matter **9**, 3107 (1997).
[80] L. C. Snyder, R. Wu, and P. Deák, Radiat. Eff. Defects Solids **111&112**, 393 (1989).
[81] B. Pajot and B. Cales, in *Oxygen, Carbon, Hydrogen and Nitrogen in Crystalline Silicon* (Ref. 7), p. 39.
[82] However, the third of the delocalized LV modes at 537 cm^{-1} is slightly of a localized oxygen-induced-silicon-mode type in the sense that the amplitude of O_i is almost vanishing and one of the Si atoms neighboring O_i and one of its Si neighbors have amplitudes which are larger than the amplitudes of the other Si atoms.
[83] In the calculated delocalized oxygen-induced silicon mode at 537 cm^{-1} the replacement of one of the neighboring Si atoms by ^{29}Si causes an isotopic shift of 0 or 1 cm^{-1} (depending on the neighbor) and the replacement of both neighboring Si atoms by ^{29}Si causes a shift of 1 cm^{-1}.
[84] M. Pesola, J. von Boehm, and R. M. Nieminen, Phys. Rev. Lett. **82**, 4022 (1999).
[85] T. Hallberg, J. L. Lindström, L. I. Murin, and V. P. Markevich, Mater. Sci. Forum **258-263**, 361 (1997).
[86] J. L. Lindström and B. G. Svensson, in *Oxygen, Carbon, Hydrogen, and Nitrogen in Crystalline Silicon* (Ref. 7), p. 45.
[87] F. A. Abou-el-Fotouh and R. C. Newman, Solid State Commun. **15**, 1409 (1974).
[88] J. Svensson, B. G. Svensson, and J. L. Lindström, Appl. Phys. Lett. **49**, 1435 (1986).
[89] H. J. Stein, Mater. Sci. Forum **10-12**, 935 (1986).